Desalination and Water Treatment
www.deswater.com

doi: 10.1080/19443994.2013.791782

51 (2013) 7120–7129
November

Taylor & Francis
Taylor & Francis Group

Characterization and Congo Red uptake capacity of a new lignocellulose/organic montmorillonite composite

Minmin Wang[a], Li Wang[a,*], Aiqin Wang[b]

[a]*College of Material Science and Art Design, Inner Mongolia Agricultural University, Huhhot 010018, China*
Tel. +86 15124706859; email: wl2083663@126.com
[b]*Center of Eco-material and Green Chemistry, Lanzhou Institute of Chemical Physics, Chinese Academy of Sciences, Lanzhou 730000, P.R. China*

Received 27 December 2011; Accepted 17 February 2013

ABSTRACT

The lignocellulose/organic montmorillonite (LNC/OMMT) composite was prepared by intercalation reaction. The samples were characterized by FTIR, X-ray diffraction, transmission electron microscopy (TEM), energy dispersive x-ray spectroscopy, and spectroscopy scanning electron microscope. The results indicated that the LNC molecules may have different influences on physico-chemical properties of OMMT; an intercalated–exfoliated structure was formed. The effects of different adsorption temperature, initial pH value of the dye solution, adsorption time, and initial concentration of dye on adsorption capacities of samples for Congo Red dye have been investigated. Compared with the maximum adsorption capacity of LNC/MMT composite (51.16 mg/g), LNC/OMMT composite exhibited a higher adsorption capacity (102.32 mg/g). The adsorption kinetics and isotherms were also studied. It was shown that all the sorption processes were better fitted by pseudo-second-order equation and Langmuir equation. Desorption studies suggest that LNC/OMMT composite exhibited a certain extent of regeneration ability.

Keywords: Lignocellulose; Organic montmorillonite; Composite; Adsorption; Desorption

1. Introduction

Nowadays, large amounts of dyes can be synthesized and used for many industries, such as textiles, paper, leather, plastics, etc [1]. Most of them are well-known toxic and carcinogenic agents and represent a serious threat to human populations as well as the fauna and flora of receiving water bodies, when discharged in wastewater [2] For example, Congo red (CR), (1-naphthalenesulfonic acid, 3,30-(4,40-biphenylenebis(azo)) bis(4-amino-)disodiumsalt) is a benzidine-based anionic diazo dye [3]. It is known to metabolize to benzidine, a known human carcinogen [4]. Therefore, it is necessary to remove the dye pollutions [5]. However, dyes usually have a synthetic origin and complex aromatic molecular structures, which make them more stable and more difficult to biodegrade and photodegrade [6]. Thus, colored wastewater poses a challenge to the conventional wastewater treatment techniques. Several methods are available for color removal from wastewater, such as membrane separation [7], adsorption [3], electrocoagulation [8], chemical oxidation [9], and coagulation and flocculation [10]. Among these

*Corresponding author.

methods, adsorption has been found to be one of the most popular physico-chemical treatment methods for removing dyes with potential applications [11]. Adsorption is done using different kinds of adsorbents [12,13], such as orange peel [14], fly ash, chitosan, and activated carbon [15]. The use of activated carbon as an adsorbent is still very popular because of its extended surface area, micro-porous structure, high adsorption capacity and high degree of surface reactivity. However, regeneration or reuse of carbon results in steep reduction in performance, and efficiency becomes unpredictable or dependent on massive carbon dosages [16]. Therefore, various low-cost and reusable adsorbents have been studied for dye removal from wastewater [17]. Currently, cellulose and montmorillonite (MMT) clay are being greatly exploited. Cellulose, the most abundant renewable polysaccharide on earth, is produced by nature at a rate of $1{,}0^{11}$–$1{,}0^{12}$ ton/year [18]. It is an inexhaustible source of raw material for environmentally friendly and biocompatible products [19]. Lignocellulose (LNC) is one of the cellulose. Because its molecules contain a large number of active hydroxyl (–OH), it is noted that cellulose has been used as sorbents for dyes [20,21] and heavy metal [22,23]. However, the poor solubility of cellulose in water and most organic solvents, poor reactivity, and adsorbing of very small amounts of dyes make it difficult to be directly used [24]. Meanwhile, the use of MMT in wastewater treatment has received increasing attention and currently offers a very attractive method for pollution remediation [25]. For example, Lin et al. reported the removal of xanthene basic dye, Rhodamine6G [26], disazo acid dye, Amido black 10B [27], disazo acid dye, and Methyl Orange 52 [28] by HCl-activated MMT SAz-1 in fixed beds. MMT is one of the clay minerals and consists of hydrated aluminum silicates with fine grains and large spaces between the layers [29]. It is characterized by both high adsorptive capacity and surface area [30]. However, natural MMT adsorbs the anionic dyes only onto the external broken bonds surface in very small amounts and difficult to compatible with organic polymeric material. Therefore, it is often needed to render the hydrophilic MMT in order to improve their adsorption capacities and increase its compatibility [31]. For these reasons, most of the investigations have been concentrated on the organic montmorillonite (OMMT) whose surface is modified to be more hydrophobic by replacing interlayer cations with organic cations [32]. For example, Hassina Zaghouane-Boudiaf and Mokhtar Boutahala have studied the equilibrium and kinetics of 2,4,5-trichlorophenol adsorption onto organophilic bentonite [33]. Therefore, OMMT can be used to adsorb organic anionic dyes such as CR.

In recent years, the expansion of industrial and economic activities demand new, effective, low-cost materials to meet increasing stringent conditions. Polymer/clay nanocomposites, as a very promising alternative to conventional filled polymers, have attracted considerable attention of academic and industrial researchers [34]. They are a new class of organic polymer materials, which serve as novel composite materials [35,36]. However, reports on the removal of dyes using The lignocellulose/organic MMT (LNC/OMMT) composite as an adsorbent are very scarce. Therefore in this study, a novel adsorbent, LNC/OMMT composite, was synthesized and characterized. The effects of various adsorption conditions, such as different adsorption temperature, adsorption time, initial concentration of the dye solution, and initial solution pH were studied. The adsorption kinetics and CR dye from water solution onto composite have been investigated.

2. Experimental

2.1. Materials

Ca-MMT (the cationic exchange capacity (CEC) is 100 mequiv/100 g) was supplied by ChiFeng of Inner Mongolia XingLong Binder HuaGong Co.(Inner Mongolia, China).Chemical analysis of MMT was performed by the PANalytical Company with a Magi-xPW2403 XRF Spectrometer, and the results are shown in Table 1. Cetyl three methyl brominated ammonium (CTAB; molecular weight of CTAB is 364.45 g/mol) was supplied by TianJin JingXi chemical research institute (TianJin, China). LNC was purchased from BeiJing QinLiHengTong Technology Co., Ltd. (BeiJing, China). CR (molecular weight of CR is 696.66 g/mol) was purchased from BeiJing Dye Co. (BeiJing, China). Other agents used were all of analytical grade, and all solutions were prepared with distilled water.

2.2. Preparation of OMMT

The synthesis of OMMT (CEC is 113 mequiv/100 g) was conducted by the following procedure. 2.73 g of CTAB was first dissolved in 82.00 mL distilled water and then 5.0 g MMT was slowly added. The reaction mixture was stirred continuously at room temperature for 12 h. The mixture was filtered and washed several times with distilled water until no bromide ion was detected by $AgNO_3$ solution (0.1 M).

Table 1
Chemical composition of MMT

Component	SiO_2	Al_2O_3	MgO	Fe_2O_3	CaO	K_2O	Na_2O	Ti	Mn
Weight(%)	71.25	13.76	5.96	5	2.75	0.24	0.07	0.21	0.02

The OMMT was dried in an air oven at 105 °C for 6 h and ground to 200 mesh size.

2.3. Preparation of LNC/OMMT composite

1.0 g of OMMT was swelled by 30 mL distilled water. LNC solution was prepared by dissolving 4.0 g LNC in 10 wt.% NaOH solution (120 mL) and stirring for 30 min; then, the LNC solution was slowly added to OMMT suspension, followed by stirring at 50 °C for 6 h to obtain the composite. The formed composite was washed with distilled water until the pH of the supernatant reached 7.00, and then dried at 105 °C for 12 h. All samples as adsorbents were ground and sieved through 200 meshes.

2.4. Adsorption experiments

All batch adsorption experiments were performed on a thermostated shaker (SHA-C) with a shaking of 120 rpm. The effect of temperature on dye removal was carried out in 25.00 mL of dye solution (500 mg/L, pH 10) with 0.10 g of adsorbent until equilibrium was established. The influence of pH on CR removal was studied by adjusting CR solutions (500 mg/L) to different pH values (4, 6, 8, 10, and 12) using a pH meter (PB-10) and agitating 25.00 mL of dye solution with 0.10 g of adsorbent at 30 °C for 360 min. The effect of time on dye removal was carried out in 25.00 mL of dye solutions (500 mg/L, pH 10) with 0.10 g of adsorbent. The effect of initial concentration of CR solution experiments, 0.10 g of the composite and 25.00 mL of CR solutions (30 °C, pH 10), were used. For kinetic study, 500 mg/L dye solutions (25.00 mL, pH 10) were agitated with 0.10 g of adsorbent at 30 °C for predetermined intervals of time, respectively. Batch equilibrium adsorption experiments were carried out by agitating 25.00 mL of CR solution of various concentrations at pH 10 with 0.10 g of adsorbent at 30 °C for 360 min, respectively. After a shaking time was completed, the suspension was separated from the adsorbent by centrifugation at 6,000 rpm for 5 min. The absorbencies of the dye solution were measured using a UV–vis spectrophotometer at a wavelength 500 nm (CR has maximum absorbency at the wavelength of 500 nm on a UV–vis spectrophotometer). Then, the concentrations of the dye solutions were determined using linear regression equation ($y = 0.0593 \times -0.041$, $R^2 = 0.9999$), obtained by plotting a calibration curve for dye over a range of concentrations.

2.5. Desorption studies

The adsorbent that was used for the adsorption of dye solution was separated from solution by centrifugation and then dried. The experiments were carried out in 25 ml NaOH (0.1 mol/L) solution and the temperature was controlled at 30 °C. The sorbent was added to the solution and simultaneously the ultrasonic power was turned on. The effects of different time on CR desorption were studied. After desorption time was completed, the suspension was separated from the adsorbent by centrifugation at 6,000 rpm for 5 min. The final CR concentrations in solution were analyzed.

2.6. Characterization

The surface area and pore size of the samples were measured using an Accelerated Surface Area and Porosimetry System (Micromeritics, ASAP2010) by BET method at 76 K. IR spectra of the samples were characterized using a FTIR spectrophotometer (Thermo Nicolet, NEXUS, TM) in KBr pellets. XRD analyses of the powdered samples were performed using an X-ray powder diffractometer with Cu anode (PANalytical Co. X'pert PRO), running at 40 kV and 30 mA, scanning from 3° to 18° at 3°/min. The morphology of transmission electron microscopy (TEM) (JEOL, Ltd., JSM-5600LV) was used at an acceleration voltage of 80 kV. Elemental analysis was taken by energy dispersive x-ray spectroscopy (EDS) (INCA system, made by Oxford Instruments). Micrographs of the samples were taken using spectroscopy scanning electron microscope (SEM) (JSM-5600LV, JEOL Ltd.). Before the observation of SEM, all samples were fixed on aluminum stubs and coated with gold. Thermal analysis of samples have been carried out at heating rate of 3 °C/min up to temperature range of 500 °C (NETZSCH-Ger tebau GmbH, STA 409PC) analyzer. The ultrasonic (KS-300EI) irradiation was carried out with equipment operating at 40 kHz.

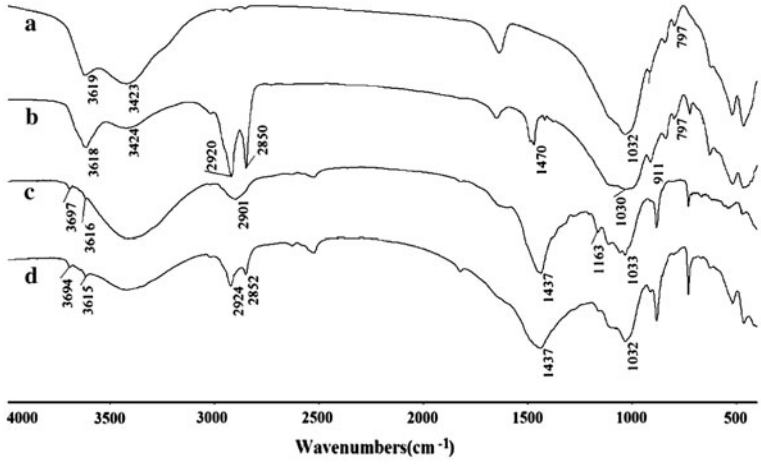

Fig. 1. IR spectra of MMT (a), OMMT (b), LNC (c) and composite (d).

3. Result and discussion

3.1. IR analysis of the composites

Fig. 1 shows IR spectra of MMT (a), OMMT (b), LNC (c), and composite (d). Compared with the IR spectra of MMT, the intense peak around 797 and 1,030 cm^{-1} corresponds to Si–O bonds' stretching. The adsorption bands around 3,424 and 3,618 cm^{-1}, assigned to –OH stretching vibration of H_2O of OMMT, strengthened and shifted to wave number 3,424 and 3,618 cm^{-1} [37] (Fig. 1(b)). The other additional bands observed in the spectrum of the OMMT arise from surfactant bonds' stretching or bending. The characteristic absorption bands of the symmetric and asymmetric stretching vibrations of $–CH_2$ (2,880 cm^{-1}) and $–CH_3$ (2,920 cm^{-1}) of intercalated CTAB were observed on the IR spectra of OMMT (Fig. 1(b)). The result indicated that the CTAB molecules may have intercalated into the space of MMT. The conclusion will be further proved by XRD, as shown in Fig. 2.

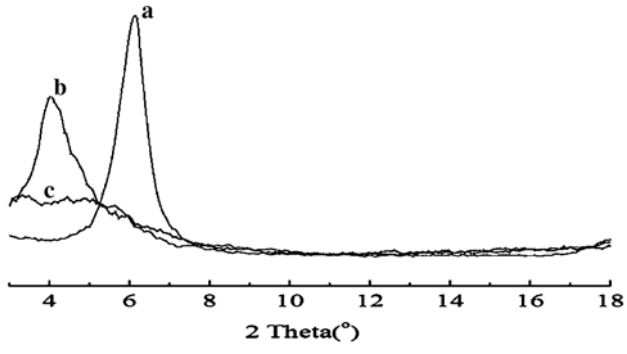

Fig. 2. XRD powder patterns of the MMT (a), OMMT (b) and composite (c).

IR spectra of pure LNC (c) and LNC/OMMT composite (d) are presented in Fig. 1. The characteristic absorption bands of OMMT due to telescopic vibrating of Mg–O–H and Al–O–H (797 and 911 cm^{-1}) disappeared in the spectra of the composite. At the same time, the bands at 1,163 and 1,437 cm^{-1} due to –C–O–C– symmetrical and antisymmetry telescopic vibration and $–CH_2$ bending vibration in LNC (Fig. 1 (c)) were observed. In addition, the adsorption band at 3,697 and 3,616 cm^{-1} assigned to –OH bending vibration of H_2O of the LNC, widened and shifted to lower wave number of 3,694 and 3,615 cm^{-1} (Fig. 1 (d)). The information observed from IR spectra indicates that LNC molecules could influence chemical environment of OMMT and may have an influence on absorption properties of the composite, which will be discussed in the following sections in detail.

3.2. X-ray diffraction analysis of the composites

X-ray diffraction (XRD) is an effective method for the investigation of the intercalation existence of MMT. The XRD patterns of MMT (a), OMMT (b) and composite (c) are presented in Fig. 2. We can notice that a typical diffraction peak of MMT was at 6.12°, responding to a basal spacing of 1.41 nm. MMT showed typical nanostructure features. Meanwhile, OMMT shows a typical diffraction peak at $2\theta = 4.52°$, which is assigned to the interlayer platelet spacing of 19.09 nm. However, after intercalation with LNC, this peak shifts to lower angle and even disappears. This indicates that LNC intercalated into OMMT interlayer. According to the results of FTIR and XRD, it can be concluded that an intercalated–exfoliated structure may have formed in the LNC/OMMT composite.

3.3. TEM images analysis of the composite

More direct evidence of the morphology of true composite was provided by TEM. It is a powerful method to combine XRD and TEM when characterizing the structure of polymer/clay composites. Fig. 3 shows the TEM microphotographs of LNC/OMMT composite. It can be seen that the dark lines in the photograph are the intersections of the clay sheets, and the spaces between the dark lines are LNC materials. Almost all LNC materials were embedded within OMMT interlayer with the destruction of the crystalline structure of OMMT, polymer matrix was well dispersed in the clay layers. Although some of the clays were agglomerate, the average particle size was found to be below 50 nm in thickness. These phenomena indicated that the disordered intercalated–exfoliated structure still existed in the composite. This was also confirmed with ESD, as shown in Fig. 4.

3.4. EDS analysis of the composite

The EDS attached to TEM was used to focus the electron beam on the composite phase and characteristic X-rays were then recorded. According to the EDS graph of the dark line(Fig. 4(a)) and its corresponding Table 3, the atomic percentages of O, Si, C, Al, Mg, Fe, and K were determined to be 43.67, 22.47, 9.74, 8.2, 3.21, 1.19, and 1.01%, respectively. Meanwhile, the EDS graph of the light phase (Fig. 4(b)) and its corresponding Table 4 showed the atomic percentages of C and O as 87.00 and 7.32%, respectively. Herein, the Cu signal was recorded due to the sample grid which was made by "Cu." In this way, EDS symbolized that the dark phase observed by TEM was mainly OMMT and the light phase was mainly LNC. The conclusion was further confirmed by the following SEM analysis.

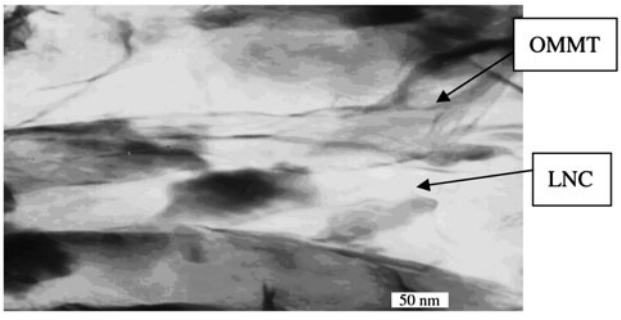

Fig. 3. TEM image of the composite.

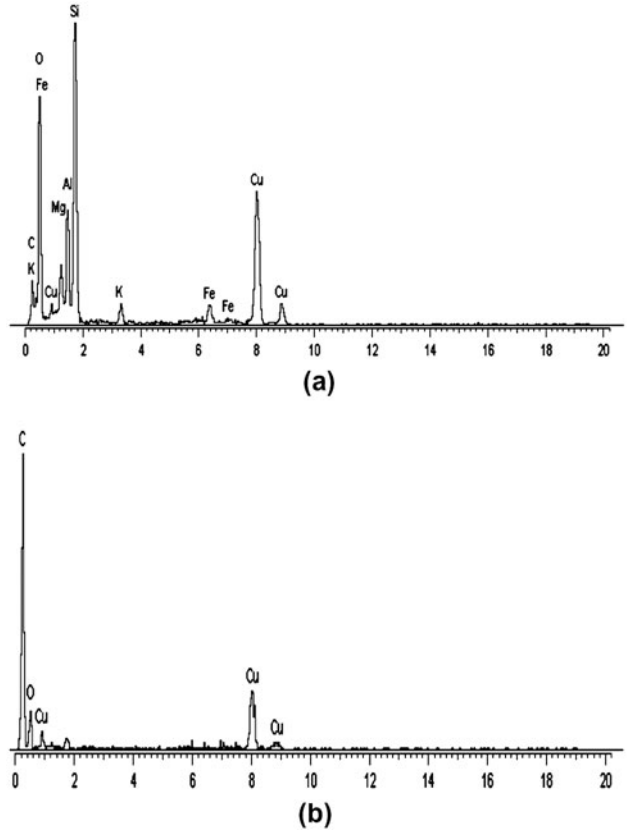

Fig. 4. EDS showing the identification of different elements in surface area of composite.

3.5. SEM images analysis of the composite

Fig. 5 shows the SEM images of MMT (a) and LNC/OMMT composite (b). We can see that the pristine MMT particles display comparative density and a flat and stretched surface. But the introduction of LNC molecules destroyed the crystalline structure of MMT; large particles having coarse, porous, and relatively loose surface was formed. This structure may be convenient for the penetration of dye molecules, and result in an increase in the adsorption capacity of CR. Table 2 can further support the explanation mentioned above.

3.6. Effect of temperature on adsorption

The effect of temperature on adsorption capacity of LNC/OMMT composite is shown in Fig. 6. As can be seen, the adsorption capacity of CR changed from 93.67 to 98.96 mg/g, with change in temperature from 20 to 30 °C; and the adsorption capacity decreased to 91.83 mg/g, when the temperature increased to 60 °C. The phenomenon indicated that the adsorption behavior is insensitive to the changes in temperature. The overall temperature influence is weak for the adsorption of CR, which probably indicates the low

Table 2
The surface and pore size of MMT, OMMT, LNC and composite

Samples	Specific surface area (m^2/g)	Average pore width (nm)
MMT	47.83	8.81
OMMT	6.67	17.03
LNC	2.89	10.19
Composite	5.72	11.07

activation energy in the predominantly ionic system [38]. Meanwhile, the temperature effect can be rather complex because of the simultaneous influence on several properties such as solvent power, polymer configuration, mineral solubility, and electrostatic adsorption [39].

3.7. Effect of solution pH

The effect of solution pH on adsorption capacity of LNC/OMMT composite was investigated and shown in Fig. 7. It can be seen that the adsorption capacity of CR on LNC/OMMT decreased from 105.32 to 99.11 mg/g with increasing pH from 4 to 6; adsorption capacity slowly reduced with further increasing of pH from 6 to 12. The result may attribute to the fact that neutralization reaction happened between anion dye molecules and hydrogen ions in solution. The slight decrease in adsorption may be due to the repulsion between anionic dye molecules and the excessive hydroxyl ions at alkaline pH values [40]. Despite this fact, adsorption of anionic dye molecules on the composite surface occurs in the whole range of pH, even at the highest values of pH. Comparatively high adsorption capacity of the anionic dye on the adsorbent occurred at pH 4.0.

3.8. Effect of time on adsorption

Fig. 8 illustrates the effect of adsorption time on the dye adsorption of CR by LNC/OMMT composite. It is clear that the adsorption capacity of the composite increased rapidly in the initial stages of adsorption time and gradually increased with prolonging the adsorption time until equilibrium. It can be seen that adsorption equilibrium of CR on the composite was reached at 360 min. So, in the test, we choose an adsorption time of 360 min to obtain the adsorption isotherms, which make sure that the adsorption equilibrium is reached.

Table 3
Element analysis of OMMT

Element	Weight %	Atomic %
C K	4.64	9.74
O K	27.73	43.67
Mg K	3.10	3.21
Al K	8.78	8.20
Si K	25.05	22.47
K K	1.57	1.01
Fe K	2.64	1.19
Cu K	26.48	10.50

Table 4
Element analysis of LNC

Element	Weight%	Atomic %
C K	68.61	87.00
O K	7.69	7.32
Cu K	23.69	5.68

3.8.1. Adsorption kinetics

In order to investigate the adsorption process of CR on the composite, pseudo-first-order and pseudo-second-order kinetic models were used. The two equation models are described as follows:

$$\frac{dq_e}{dt} = k_1(q_e - q_t) \quad (1)$$

$$\frac{dq_e}{dt} = k_2(q_e - q_t)^2 \quad (2)$$

where k_1 is the pseudo-first-order rate constant (min^{-1}) and q_e and q_t are the amounts of dye adsorbed (mg/g) at equilibrium and at time t (min). k_2 ($g\,mg^{-1}\,min^{-1}$) is the rate constant of the pseudo-second-order adsorption.

The rate constants k_1 and k_2 can be obtained from the plot of experimental data. The rate constants and the correlation coefficients of the two kinetic models are shown in Table 5. The correlation coefficients (R^2) of the pseudo-first-order and pseudo-second-order models are 0.8939 and 0.9983 for the composite, respectively. It can be seen that the adsorption of CR is in good agreement with pseudo-second-order model rather than pseudo-first-order model. These results indicated that the adsorption rate of CR dye depended on the concentration of dye at the adsorbent surface and the absorbance of these absorbed at equilibrium [40]. In addition, theoretical calculation value (q_e) of the pseudo-first-order and pseudo-second-order for

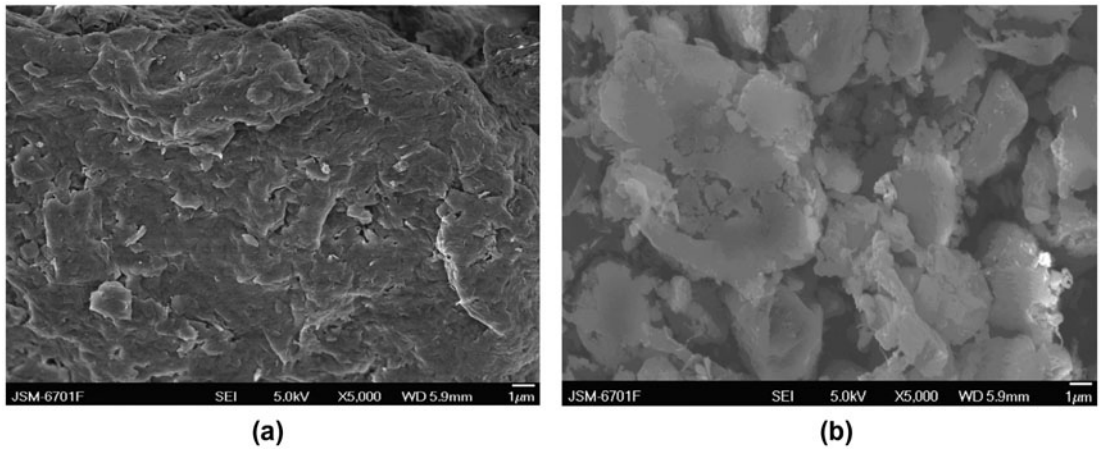

Fig. 5. SEM image of MMT (a) and composite (b).

the adsorption of CR by LNC/OMMT are 47.09 and 104.17 mg/g, respectively. Obviously, 104.17 mg/g is close to the experimental data (98.96 mg/g) in the case of the pseudo-second-order model. Compared with q_e values of the pseudo-second-order model by LNC/MMT composite (52.14 mg/g), LNC/OMMT composite exhibited higher adsorption capacity.

3.9. Effect of the initial concentration of dye on adsorption

Initial dye concentration is an important factor that affects the adsorption capacity of the composite. Fig. 9 shows the adsorption capacity of CR by the composite at different dye concentrations. It is clear that the adsorption capacity of the composite increased sharply from 68.14 to 98.96 mg/g with increase of dye concentration from 300 to 500 mg/L. However, only a slight increase in the adsorption capacity of the composite can be observed with further increasing the initial concentration of dye; Jiangtao Zhu et al. have got the same experimental phenomenon [41]. This may be attributed to the fact that the aggregation of CR dye molecules makes it almost impossible for them to diffuse deeper into the composite structure [42].

3.9.1. Adsorption isotherms

In order to investigate the adsorption process of CR on the adsorbent, two adsorption isotherms described the relationship between the amount of adsorbate adsorbed on the adsorbent and the concentration of dissolved adsorbate in the liquid at equilibrium.

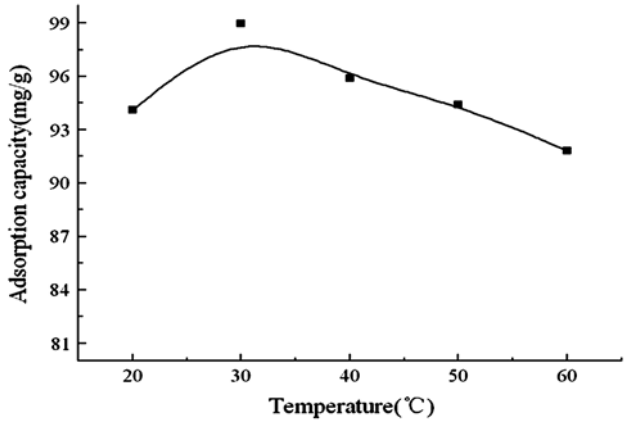

Fig. 6. Effect of the temperature on adsorption capacity of LNC/OMMT composite for CR. Adsorption experiments – dye concentration: 500 mg/L; sample dose: 0.10 g/25.00 mL; pH = 10; temperature: 20–60 °C; equilibrium time: 360 min.

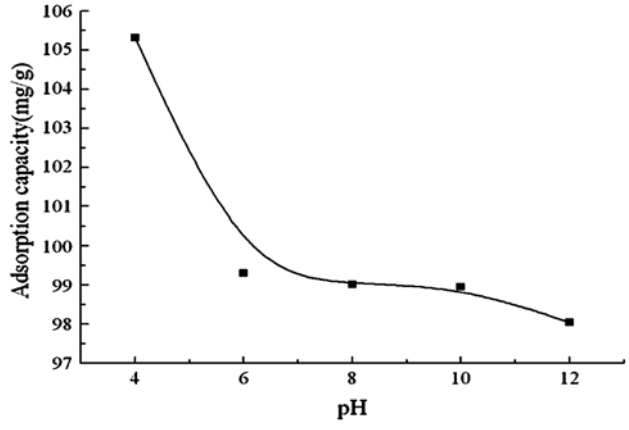

Fig. 7. Effect of solution pH on adsorption capacity of LNC/OMMT for CR. Adsorption experiments-dye concentration: 500 mg/L; sample dose: 0.10 g/25 mL; pH range: 4–12; temperature: 30 °C; equilibrium time: 360 min.

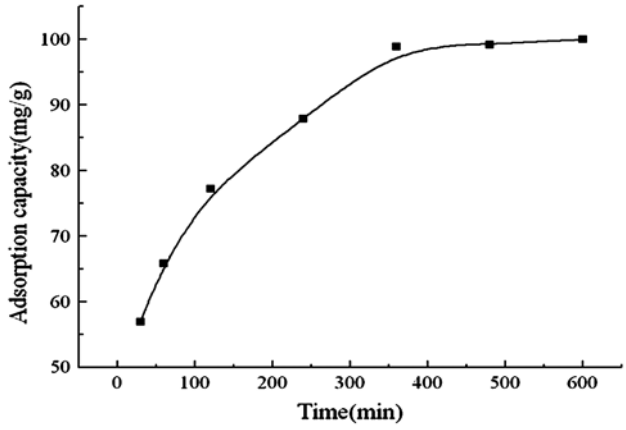

Fig. 8. Effect of the adsorption time on adsorption capacity of LNC/OMMT composite for CR. Adsorption experiments – dye concentration: 500 mg/L; sample dose: 0.10 g/25.00 mL; pH = 10; time: 30–600 min; temperature: 30 °C.

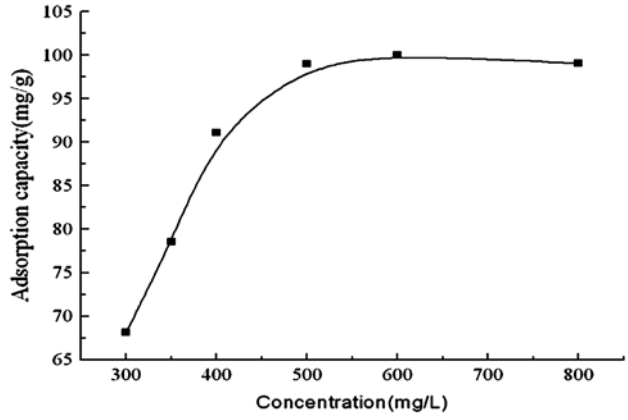

Fig. 9. Effect of the dye concentration on adsorption capacity of LNC/OMMT composite for CR. Adsorption experiments – sample dose: 0.10 g/25.00 mL; pH = 10; adsorption temperature: 30 °C; equilibrium time: 360 min; initial concentration: 300–1,000 mg/L.

Results obtained from the adsorption isotherm were evaluated by means of Langmuir and Freundlich adsorption models. The Langmuir and Freundlich equations are represented as follows, respectively:

$$\frac{C_e}{q_e} = \frac{C_e}{q_m} + \frac{1}{q_m K_1} \tag{3}$$

$$q_e = K_f C_e^{\,1/n} \tag{4}$$

where C_e is the equilibrium concentration of the dye (mmol/L); q_e is the adsorbed value of dyes at equilibrium concentration (mmol/g); K_1 is the Langmuir binding constant which is related to the energy of adsorption (L/mmol); q_m is the Langmuir maximum adsorption capacities of the dye (mmol/g); and K_f (mg/g) is Freundlich constants related to the adsorption capacity.

The essential characteristics of Langmuir isotherm can be expressed by a dimensionless constant called equilibrium parameter R_L that is defined by the following equation:

$$R_L = \frac{1}{1 + bC_0} \tag{5}$$

where b (mg^{-1}) is the Langmuir constant related to the energy of adsorption and C_0 is the initial concentration. The value of R_L is calculated from the above expression. The nature of the adsorption process is found to be unfavorable ($R_L > 1$), linear ($R_L = 1$), favorable ($0 < R_L < 1$), or irreversible ($R_L = 0$).

The constants (K_1 and K_f) and the correlation coefficients of the two isotherms models are shown in Table 6. We can see that the correlation coefficient (R^2) was found as 0.9999 and 0.6192, respectively. In addition, theoretically calculated value (q_e) of Langmuir adsorption model for the adsorption of CR by LNC/OMMT was 102.04 mg/g. The value was confirmed to be in very good agreement with the experimental data (98.96 mg/g). It can be concluded that Langmuir model fitted the adsorption isotherms better than the Freundlich model. Thus, LNC/OMMT composite is useful as a promising adsorbent for the removal of CR dye in wastewater treatment.

3.10. Effect of ultrasonic waves time on desorption of CR

Fig. 10 presented the removal of CR by ultrasonic wave from sorbent. As it was shown, about 45% of the adsorbed CR was removed by desorption after 20 min in the ultrasonic wave. However, the desorption

Table 5
The rate constants and the correlation coefficients of the two kinetic models

Pseudo-first-order model		Pseudo-second-order model	
$K_1(\times 10^{-2}\,min^{-1})$	R_1^2	$K_2(\times 10^{-4}\,g/mg/min)$	R_2^2
1.59	0.8939	2.86	0.9983

Table 6
The constants and the correlation coefficients of the two isotherms models

Langmuir			Freundlich	
K_1 (mg/l)	R_1^2	R_L	K_f (mg/l)	R_2^2
0.1355	0.9990	0.0145	53.7208	0.6192

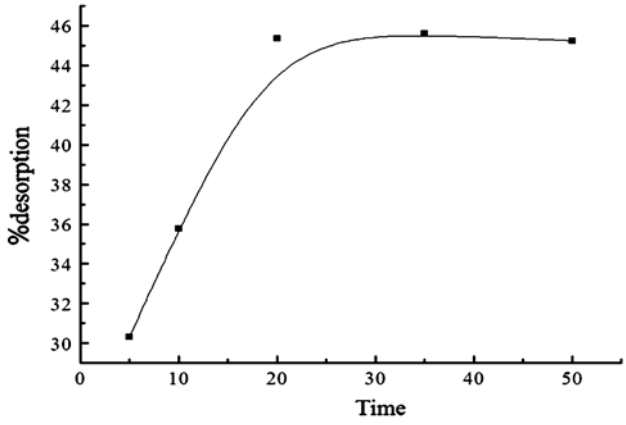

Fig. 10. Effect of ultrasonic wave time on the dye removal in absence of sorbent. Desorption experiment—; sample dose: 0.10 g/25 mL; temperature: 30 °C.

efficiency hardly increased with further increase in time. The phenomenon responsible for this reduction is the formation of hydroxyl radical during sonication of aqueous solution by the cavitation process. This process consists of the formation, growth, and collapse by violent implosions to release pressures at local hot spots in the liquid [43]. However, the chemisorptive adsorption of CR onto the composite hindered the desorption. The experimental result indicated that the LNC/OMMT composite exhibited a certain extent of regeneration ability.

4. Conclusion

A novel composite was synthesized by intercalation reaction between LNC and OMMT. FT-IR, XRD, TEM, EDS, and SEM analysis indicated that an intercalated–exfoliated structure was formed in LNC/OMMT composite. Adsorption tests of CR dye on LNC/OMMT composite were carried out and the results showed that the CR dye adsorption process is dependent on the temperature and the solution pH. The adsorption kinetics obeys the pseudo-second-order model and the isotherm follows the Langmuir monolayer model. LNC/OMMT composite is comparatively low cost and has relatively high adsorption capacity. The LNC/OMMT composite showed a certain extent of regeneration ability of up to 45.76%. Therefore, the composite can be effectively used as an adsorbent for the removal of CR from wastewater.

Acknowlegments

This work was financially supported by Special Fund for National Forestry Industry Scientific Research in the Public Interest of China (No. 201104004), the Natural Science Foundation of Inner Mongolia (No.2012MS0606), and program for young talents of science and technology in universities of Inner Mongolia autonomous region.

References

[1] L. Wang, J.P. Zhang, A.Q. Wang, Fast removal of methylene blue from aqueous solution by adsorption onto chitosan-g-poly (acrylic acid)/attapulgite composite, Desalination 266 (2011) 33–39.
[2] T.N.C. Dantas, A.A.D. Neto, M.C.P.A. Moura, E.L.B. Neto, E.P. Telemaco, Chromium adsorption by chitosan impregnated with microemulsion, Langmuir 17 (2001) 4256–4260.
[3] I.D. Mall, V.C. Srivastava, N.K. Agarwal et al., Removal of congo red from aqueous solution by bagasse fly ash and activated carbon: Kinetic study and equilibrium isotherm analyses, Chemosphere 61 (2005) 492–501.
[4] O.J. Hao, H. Kim, P.C. Chiang, Decolorization of wastewater, Crit. Rev. Environ. Sci. Technol. 30 (2000) 449–505.
[5] H. Chen, J. Zhao, Adsorption study for removal of Congo red anionic dye using organo-attapulgite, Adsorption 15 (2009) 381–389.
[6] V.K. Gupta, A. Mittal, L. Kurup, J. Mittal, Adsorption of a hazardous dye, erythrosine, over hen feathers, J. Colloid Interface Sci. 304 (2006) 52–57.
[7] G. Ciardelli, L. Corsi, M. Marucci, Membrane separation for wastewater reuse in the textile industry, Resour. Conserv. Recycl. 31 (2000) 189–197.
[8] A. Alinsafi, M. Khemis, M.N. Pons, J.P. Leclerc, A. Benhammou, A. Nejmeddine, Electro-coagulation of reactive textile dyes and textile wastewater, Chem. Eng. Process. 44 (2004) 461–470.
[9] K. Swaminathan, S. Sandhya, S.A. Carmalin, K. Pachhade, Y.V. Subrahmanyam, Decolorization and degradation of Hacid and other dyes using ferrous–hydrogen peroxide system, Chemosphere 50 (2003) 619–625.
[10] J. Panswed, S. Wongchaisuwan, Mechanism of dye wastewater color removal by magnesium carbonate-hydrated basic, Water Sci. Technol. 18 (1986) 139–144.
[11] A.S. Özcan, A. Özcan, Adsorption of acid dyes from aqueous solutions onto acidactivated bentonite, J. Colloid Interface. Sci. 276 (2004) 39–46.
[12] O.J. Hao, H. Kim, P.C. Chiang, Decolorization of wastewater, Crit. Rev. Environ. Sci. Technol. 30 (2000) 449–505.
[13] Y.M. Slokar, A. Majcen-Le Marechal, Methods of decoloration of textile wastewaters, Dyes Pigm. 37 (1998) 335–356.
[14] M. Arami, N. Yousefi Limaee, N. Mohammad Mahmoodi, N. Salman Tabrizi, Removal of dyes from colored textile wastewater by orange peel adsorbent: Equilibrium and kinetic studies, Colloid Interface Sci. J. 288 (2005) 371–376.
[15] J.D. Zhang, F.F. Liu, Adsorption of natural organic matter onto a composite adsorbent prepared with chitosan and powdered activated carbon, Desalin. Water Treat. 20 (2010) 291–296.
[16] C. Raghavacharya, Colour removal from industrial effluent-a comparative review of available technologies, Chem. Eng. World 32 (1997) 53–58.
[17] J.X. Lin, S.L. Zhan, M.H. Fang, X.Q. Qian, The adsorption of dyes from aqueous solution using diatomite, J. Porous Mater. 14 (2007) 449–455.
[18] D.N.S. Hon, Cellulose: A random walk along its historical path, Cellulose 1 (1994) 1–25.
[19] J. Kim, N.G. Wang, Y. Chen, Effect of chitosan and ions on actuation behavior of cellulose–chitosan laminated films as electro-active paper actuators, Cellulose 14 (2007) 439–445.
[20] M.C. Hwang, K.M. Chen, Removal of color from effluents using polyamideepichlorohydrin–cellulose polymer II: Use in acid dye removal, J. Appl. Polym. Sci. 49 (1993) 975–989.

[21] A. Hashem, R.M. EI-Shishtawy, Preparation and characterization of cationized cellulose for the removal of anionic dyes, Adsorpt. Sci. Technol. 19 (2001) 197–210.
[22] X. Guo, Y. Du, F. Chen, H.S. Park, Y. Xie, Mechanism of removal of arsenic by bead cellulose loaded with iron oxyhydroxide (β-FeOOH): EXAFS study, J. Colloid Interface Sci. 314 (2007) 427–433.
[23] E. Mīstova, H. Parschova, Z. Matějka, Selective sorption of metal oxoanions from dilute solution by bead cellulose sorbent, Sep. Sci. Technol. 42 (2007) 1231–1243.
[24] W.B. Wang, A.Q. Wang, Nanocomposite of carboxymethyl cellulose and attapulgite as a novel pH-sensitive superabsorbent: Synthesis, characterization and properties, Carbohydr. Polym. 82 (2010) 83–91.
[25] A. Khenifi, Z. Bouberka, F. Sekrane, M. Kameche, Z. Derriche, Adsorption study of an industrial dye by an organic clay, Adsorption 13 (2007) 149–158.
[26] M.Y. Teng, S.H. Lin, Removal of basic dye from water onto pristine and HCl-activated montmorillonite in fixed beds, Desalination 194 (2006) 156–165.
[27] S.H. Lin, R.S. Juang, Y.H. Wang, Adsorption of acid dye from water onto pristine and acid-activated clays in fixed beds, J. Hazard. Mater. 113 (2004) 195–200.
[28] M.Y. Teng, S.H. Lin, Removal of methylene orange dye from water onto raw and acid-activated montmorillonite in fixed beds, Desalination 201 (2006) 71–81.
[29] F.H. Lin, Y.H. Lee, C.H. Jian, J.M. Wang, M.J. Shieh, Y.W. Cheng, A study of purified montmorillonite intercalated with 5-fluorouracil as drug carrier, Biomaterials 23 (2002) 1981–1987.
[30] A. Babar, S.D. Ray, N.K. Patel, F.M. Plakogiannis, P. Gogiani, *In vitro* release and diffusion studies of promethazine hydrochloride from polymeric dermatological bases using cellulose membrane and hairless, mouse skin, Drug Dev. Ind. Pharm. 25 (1999) 235–240.
[31] M.A. Paul, M. Alexandre, P. Degée, C. Henrist, A. Rulmont, P. Dubois, New nanocomposite materials based on plasticized poly(L -lactide) and organo-modified montmorillonites: Thermal and morphological study, Polymer 44 (2003) 443–450.
[32] J.Y. Yu, M.Y. Shin, J.H. Noh, J.J. Seo, Adsorption of phenol and chlorophenols on Ca-montmorillonite in aqueous solutions, Geosci. J. 8 (2004) 185–189.
[33] H. Zaghouane-Boudiaf, M. Boutahala, Equilibrium and kinetics studies of 2,4,5-trichlorophenol adsorption onto organophilic-bentonite, Desalin. Water Treat. 24 (2010) 47–54.
[34] Y.B. Cai, Y. Hu, S.Y. Xuan, Y. Zhang, H.X. Deng, X.L. Gong, Z.Y. Chen, W.C. Fan, Preparation and characterization of poly (styrene-acrylonitrile)(SAN)/clay nanocomposites by melt intercalation, J. Mater. Sci. 42 (2007) 5524–5533.
[35] E.P. Giannelis, Polymer-layered silicate nanocomposites, Adv. Mater. 8 (1996) 29–35.
[36] Z. Wang, T.J. Pinnavaia, Nanolayer reinforcement of elastomeric polyurethane, Chem. Mater. 10 (1998) 3769–3771.
[37] M. Jaymand, Surface modification of montmorillonite with novel modifier and preparation of polystyrene/montmorillonite nanocomposite by *in situ* radical polymerization, J. Polym. Res. 18 (2010) 957–963.
[38] Q.H. Hu, S.Z. Qiao, F. Haghseresht, M.A. Wilson, G.Q. Lu, Adsorption study for removal of basic red dye using bentonite, Ind. Eng. Chem. Res. 45 (2006) 733–738.
[39] L.M. Zhang, Y.B. Tan, Z.M. Li, Adsorption of a new amphoteric cellulosic copolymer onto bentonite, Colloid Polym. Sci. 277 (1999) 499–502.
[40] L. Wang, A.Q. Wang, Adsorption behaviors of Congo red on the N, O-carboxymethyl-chitosan/montmorillonite nanocomposite, Chem. Eng. J. 143 (2008) 43–50.
[41] J.T. Jiang, Z.H. Hang, F.Y. Kang et al., Adsorption kinetics of activated bamboo charcoal for phenol, New Carbon Mater. 23 (2008) 326–330.
[42] I.D. Mall, V.C. Srivastava, N.K. Agarwal, I.M. Mishra, Removal of Congo Red from aqueous solution by bagasse fly ash and activated carbon: Kinetic study and equilibrium isotherm analyses, Chemosphere 61 (2005) 492–501.
[43] M.H. Entezari, Z. Sharif Al-Hoseini, Sono-sorption as a new method for the removal of methylene blue from aqueous solution, Ultrason. Sonochem. 14 (2007) 599–604.